Article type: Full Paper

A New Class of Organic Crystals with Extremely Large Hyperpolarizability: Efficient THz Wave Generation with Wide Flat-Spectral-Band

Seung-Jun Kim†, In Cheol Yu†, Dong-Joo Kim, Mojca Jazbinsek, Woojin Yoon, Hoseop Yun, Dongwook Kim, Fabian Rotermund, O-Pil Kwon**

S. J. Kim, D. J. Kim, Prof. O. P. Kwon
Department of Molecular Science and Technology, Ajo
u University, Suwon 16499 (Korea)
E-mail: opilkwon@ajou.ac.kr
I. C. Yu, Prof. F. Rotermund
Department of Physics, Korea Advanced Institute of Science and Technology (KAIST), Daejeon 34141 (Korea)
E-mail: rotermund@kaist.ac.kr
Dr. M. Jazbinsek
Institute of Computational Physics, Zurich University of Applied Sciences (ZHAW), 8401 Winterthur (Switzerland)
W. Yoon, Prof. H. Yun
Department of Chemistry & Department of Energy Systems Research, Ajou University, Suwon 16499 (Korea)
Prof. D. Kim
Department of Chemistry, Kyonggi University, San 94-6, Iui-dong, Yeongtong-gu, Suwonsi, Gyeonggi 443-760 (Korea)

†These authors equally contributed to this work.

Keywords: nonlinear optics, electro-optics, THz photonics

Abstract:

In organic π-conjugated crystals, enhancing molecular optical nonlinearity of chromophores (e.g., first hyperpolarizability $\beta \geq 300 \times 10^{-30}$ esu) in most cases unfortunately results in zero macroscopic optical nonlinearity, which is a bottleneck in organic nonlinear optics. In this work, we report a new class of nonlinear optical organic crystals introducing a chromophore possessing an extremely large first hyperpolarizability. With newly designed 4-(4-(4-(hydroxymethyl)piperidin-1-yl)styryl)-1-(pyrimidin-2-yl)pyridin-1-ium (PMPR) chromophore, incorporating a head-to-tail cation-anion O-H···O hydrogen-bonding synthon and an optimal selection of molecular anion into crystals results in extremely large macroscopic optical nonlinearity with effective first hyperpolarizability β_{iii}^{eff} of 335×10^{-30} esu. This is in sharp contrast to zero β_{iii}^{eff} value for previously reported analogous crystals. An ultra-thin PMPR crystal with a thickness of about 10 μm exhibits excellent THz wave generation performance. We simultaneously achieved i) broadband THz wave generation with a wide flat-spectral-band in the range of 0.7-3.4 THz defined at -3 dB and high upper cut-off generation frequency of > 7 THz, as well as ii) high generation efficiency (5 times higher THz amplitude than ZnTe crystal with a mm-scale thickness). Therefore, new PMPR crystals are highly promising materials for diverse applications in nonlinear optics and THz photonics.

1. Introduction

Nonlinear optical materials are highly attractive for diverse applications in telecommunications, integrated optics, THz wave photonics, frequency conversion, and electro-optic modulation.[1-9] A large macroscopic second-order optical nonlinearity in materials is the key parameter to achieve efficient performance in these applications. In integrated photonic devices, large macroscopic second-order optical nonlinearity allows a low operation voltage (e.g., half-wave voltage in Mach-Zehnder interferometer that is reciprocally proportional to the electro-optic coefficient).[2-4] Also for THz photonic devices, the macroscopic optical nonlinearity is a crucial material parameter. For THz wave generators based on difference frequency generation (DFG) or optical rectification (OR), THz generation efficiency is proportional to the square of the second-order nonlinear optical susceptibility $\chi^{(2)}$,[9,10] while the detection sensitivity is proportional to the electro-optic coefficient for THz detection based on optical phase detection with electro-optic sampling (EOS) or THz-induced lensing (TIL) methods.[9,11,12]

To obtain a large macroscopic optical nonlinearity in organic crystals, highly dipolar π-conjugated chromophores have to be self-assembled with a high order parameter, optimally perfectly parallel, without inversion symmetry.[1,13,14] Unfortunately, introducing chromophores having an extremely large, top-level molecular optical nonlinearity (e.g., first hyperpolarizability $\beta \geq 300 \times 10^{-30}$ esu) into crystals mostly results in centrosymmetric self-assembly of chromophores, i.e. with inversion symmetry, which leads to zero macroscopic second-order optical nonlinearity. The first hyperpolarizability of push-pull chromophores generally increases with increasing electron donating strength of electron donating groups (EDGs).[2,13,14] For instance, for *N*-pyrimidinyl stilbazolium chromophores, the maximum first hyperpolarizability β_{max} in gas phase increases with increasing the strength of EDGs in the order of 4-hydroxyphenyl, 4-hydroxy-3-methoxyphenyl, and 4-dimethylaminophenyl groups for

OPR ((4-hydroxystyryl)-1-(pyrimidin-2-yl)pyridinium), HPR (4-(4-hydroxy-3-methoxystyryl)-1-(pyrimidin-2-yl)pyridinium), and DAPR (4-(4-(dimethylamino)styryl)-1-(pyrimidin-2-yl)pyridinium) chromophores, respectively (see Scheme 1a and 1b). However, the macroscopic optical nonlinearity (which scales with the effective first hyperpolarizability β_{iii}^{eff}) in crystals decreases with increasing molecular optical nonlinearity β_{max}.[15-17] Eventually, although the DAPR chromophore introducing the strongest electron donating dialkylamino EDG exhibits the largest molecular optical nonlinearity β_{max}, DAPR crystals exhibit centrosymmetric crystal structure with zero effective first hyperpolarizability β_{iii}^{eff}.[15]

It is well known since two decades that the DAPR chromophore, consisting of *N*-pyrimidinyl stilbazolium and dialkylamino EDG, exhibits extremely large molecular optical nonlinearity that is up to several times higher than that of the benchmark 4-(4-(dimethylamino)styryl)-1-methylpyridinium 4-methylbenzenesulfonate (DAST) crystals.[15,18-20] However, DAPR and analogous crystals possessing large macroscopic optical nonlinearity have never been reported yet. Herein, to the best of our knowledge, we report the first DAPR analogous crystals that exhibit extremely large macroscopic optical nonlinearity.

In this work, we newly designed the cationic chromophore PMPR (4-(4-(4-(hydroxymethyl)piperidin-1-yl)styryl)-1-(pyrimidin-2-yl)pyridin-1-ium, Figure 1a) possessing extremely large, top-level molecular optical nonlinearity (Scheme 1b). In crystals, incorporating a head-to-tail cation-anion O-H···O hydrogen-bonding synthon and selecting an optimal molecular anion result in extremely large effective first hyperpolarizability β_{iii}^{eff} of 335 × 10^{-30} esu. This is about double the value achieved in benchmark DAST crystals with β_{iii}^{eff} = 161 × 10^{-30} esu.[20,21] Based on the large macroscopic optical nonlinearity, as-grown PMPR-based crystal with an ultra-thin thickness of about 10 μm shows excellent THz generation performance; both broadband generation with a wide flat-spectral-band and high generation efficiency. It satisfies the requirements of an ideal THz source for broadband THz spectroscopy.

Therefore, PMPR crystals are very promising materials for THz photonic and other nonlinear optical applications.

2. Results and Discussion

2.1. Design for Overcoming the Bottleneck in Nonlinear Optics

Figure 1a shows the chemical structure of the newly designed PMPR cation and two molecular counter anions, MO (4-((4-(dimethylamino)phenyl)diazenyl)benzenesulfonate) and CBS (4-chlorobenzenesulfonate). For designing the new PMPR cationic chromophore, we considered i) boosting molecular optical nonlinearity and simultaneously ii) introducing a hydrogen-bond donor group to promote a head-to-tail cation-anion O-H···O hydrogen-bonding synthon that may induce non-centrosymmetric ordering of chromophores in the crystalline state. To obtain large molecular optical nonlinearity, a strong EDG, the piperidino group on piperidin-4-ylmethanol (PM) group and a strong electron withdrawing group (EWG), the *N*-pyrimidinyl pyridinium (PR) group are introduced at the ends of the PMPR chromophore. Since PMPR and DAPR chromophores have an analogous EDG, piperidino and dialkylamino group, respectively, the PMPR chromophore is expected to possess a large molecular optical nonlinearity like the DAPR chromophore.

For achieving non-centrosymmetric ordering of PMPR chromophores in the crystalline state by incorporating a head-to-tail cation-anion O-H···O hydrogen-bonding synthon, hydrogen-bond donor and acceptor groups are introduced into cation and anion, respectively. The aliphatic hydroxyl –OH (δ+) group on PM EDG at an end of PMPR cations and the negative O atoms on aromatic sulfonate group at an end of MO (and CBS) anions can act as hydrogen-bond donor and acceptor, respectively as shown in Figure 1a.[22-25] We explore here two molecular counter anions with a different size; the bigger MO anion and the smaller CBS anion.

New PMPR-MO and PMPR-CBS were synthesized by the metathesis reaction of PMPR chloride (PMPR-Cl) and the corresponding sodium aromatic sulfonate (or silver aromatic sulfonate). The details of the synthesis, crystallization processes, and crystal structure and symmetry analysis are described in Supporting Information. PMPR-MO exhibits polymorphism at our experimental conditions; two polymorphs, PMPR-MO(I) and PMPR-MO(II) were observed as shown in Figure S1. In contrast we did not observe polymorphism for PMPR-CBS.

Although PMPR-MO and PMPR-CBS consist of an identical PMPR chromophore and an identical head-to-tail cation-anion O-H···O hydrogen-bonding synthon, their crystal symmetry can be different. It is because the molecular MO and CBS anions possess a substantially different size that may additionally contribute to interionic interactions. In qualitative powder second harmonic generation (SHG) measurements[26,27] at the fundamental wavelength of 1300 nm, PMPR-CBS powder shows no measurable SHG signal expected at 650 nm, but a clear third harmonic generation (THG) signal at 433 nm as shown in Figure S3. Two polymorphs of PMPR-MO exhibit different results; PMPR-MO(I) powder shows a strong SHG signal, while PMPR-MO(II) powder shows no SHG signal. These results indicate that PMPR-CBS and PMPR-MO(II) possess a centrosymmetric, while PMPR-MO(I) a non-centrosymmetric crystal structure with a second-order nonlinear optical functionality.

To investigate the details of the molecular ordering in PMPR-MO crystals, we grow single crystals of PMPR-MO(I) and PMPR-MO(II) phases. PMPR-MO(I) crystals exhibit non-centrosymmetric monoclinic *Pc* space group symmetry and PMPR-MO(II) crystals exhibit centrosymmetric triclinic $P\bar{1}$ space group symmetry. The corresponding molecular ordering of PMPR-MO(I) and PMPR-MO(II) crystals is presented in Figure 2 and S2, respectively. Importantly, PMPR-MO(I) crystals have an optimal molecular ordering of PMPR chromophores for second-order nonlinear optics; a (close-to) perfect parallel alignment of PMPR chromophores (Figure 2). PMPR-MO(I) crystals exhibit head-to-tail self-assembly

between PMPR cations and MO anions (Figure 1b). A pair of PMPR cationic chromophore and MO anion forms a strong hydrogen bond between the -OH···$^{-}O_3S$- groups with a very short distance of 2.23 Å. As a consequence, among three crystalline phases of PMPR-based crystals, PMPR-MO(I) crystals are highly attractive for macroscopic second-order nonlinear optical applications.

The reason of obtaining different crystal symmetry in non-centrosymmetric PMPR-MO(I) and centrosymmetric PMPR-CBS crystals may be attributed to the size of molecular anions. To explore this hypothesis, we analyze the crystallographic volume of cationic chromophores and anions in benchmark organic nonlinear optical salt crystals with high order parameter,[16,20,22-24,28-51] by using the Hirshfeld surface analysis.[52-54] The results are plotted in Figure 1c. Note that the previously reported benchmark organic nonlinear optical salt crystals having a high order parameter close to the maximum value (~1.0) can be classified into two groups; parallel- and series-type assemblies.[9] In this work, Group 1 and 2 crystals correspond to parallel- and series-type assemblies, respectively (see Figure 1c).

In parallel-type assembly in benchmark crystals, cationic chromophore layers are surrounded by anionic layers as shown in Figure 1d. Group 1 crystals are based on many cationic chromophores; DAS (4-(4-(dimethylamino)styryl)-1-methylpyridinium), OHP (4-(4-hydroxystyryl)-1-methylpyridinium), DHP (4-(3,4-dihydroxystyryl)-1-methylpyridinium), MOS (4-(4-methoxystyryl)-1-methylpyridinium), OPR, DEP (4-((4-(dimethylamino)phenyl)ethynyl)-1-methylpyridin-1-ium), 6MNEP (4-(2-(6-methoxynaphthalen-2-yl)vinyl)-1-methylpyridinium), HMQ (2-(4-hydroxy-3-methoxystyryl)-1-methylquinolinium), HMnXQ (halogenated 2-(4-hydroxy-3-methoxystyryl)-1-methylquinolinium), OHQ (2-(4-hydroxystyryl)-1-methylquinolinium), HMB (2-(4-hydroxy-3-methoxystyryl)-3-methylbenzothiazol-3-ium), OHB (2-(4-hydroxy-3-methoxystyryl)-3-methylbenzothiazol-3-ium), HMI (2-(4-hydroxy-3-methoxystyryl)-1,3-dimethyl-1H-benzoimidazol-3-ium), and OHI (2-(4-hydroxystyryl)-1,3,3-trimethyl-3H-indolium).[17,20,28-50]

Interestingly, for Group 1 crystals, the crystallographic volume of both cationic chromophores and counter anions is within a very narrow range; ~270-380 and ~180-230 Å^3, respectively.

For cationic chromophores of a larger size (e.g., PMB (2-(4-(4-(hydroxymethyl)piperidin-1-yl)styryl)-3-methylbenzothiazol-3-ium), PMQ (2-(4-(4-(hydroxymethyl)piperidin-1-yl)styryl)-1-methyl-quinolinium), and PMnXQ (halogenated 2-(4-(4-(hydroxymethyl)piperidin-1-yl)styryl)-1-methyl-quinolinium)), the assembling changed; from parallel-type assembly to series-type assembly (i.e., Group 2 in Figure 1c).[22-24,51] This shows that a proper balance between the volume of cation and anion may be needed for obtaining a high order parameter (i.e., large macroscopic optical nonlinearity).

In PMPR-MO(I) crystals, PMPR cation layers are surrounded by MO anionic layers (Figure 1e). This is a typical feature of parallel-type assembly. In PMPR-MO(I) crystals, PMPR cationic chromophore possesses a much bigger crystallographic volume (482 Å^3) compared to the cationic chromophores in Group 1 (~270-380 Å^3). For surrounding PMPR cations by anions, longer MO anions compared to CBS anions may be advantageous for formation of parallel-type assembly. If PMPR cations were surrounded by small CBS counter anions in the formation of parallel-type assembly, CBS anion layers could not fully surround PMPR cationic layers, which would result in many empty spaces in crystals, i.e., an unfavorable molecular ordering in the crystalline state. Therefore, PMPR-MO(I) crystals having parallel-type assembly present a new class of organic crystals having top-level macroscopic optical nonlinearity; different to previously reported benchmark crystals (Group 1 and 2 in Figure 1c).

2.2. Extremely Large Macroscopic Hyperpolarizability

As mentioned above, the PMPR chromophore is an analogue to the DAPR chromophore. The DAPR cationic chromophore exhibits a very large molecular optical nonlinearity; e.g., the first hyperpolarizability β_{HRS} of 1015 × 10^{-30} esu obtained from hyper-Rayleigh scattering (HRS) in acetonitrile solution at 1300-nm fundamental wavelength[18] and the maximum (non-

resonant) first hyperpolarizability β_{max} of 281 × 10^{-30} esu as evaluated in this work (Scheme 1). Therefore, the PMPR cationic chromophore is also expected to possess a large molecular optical nonlinearity. In addition, since PMPR-MO(I) crystals exhibit a (close-to) perfectly parallel ordering of PMPR chromophores, they must possess a large macroscopic optical nonlinearity. In this work, to evaluate the macroscopic optical nonlinearity of PMPR-MO(I) crystals, we calculated the maximum first hyperpolarizability β_{max} of PMPR chromophore having an optimized conformation (OPT) using density functional theory calculations and then consider the orientation of PMPR chromophores in the crystalline state.[21,37] The details are described in Supporting Information. In previous reports, this method has shown a good agreement with experimental macroscopic nonlinear optical response.[30,55]

Figure 3a shows the frontier molecular orbitals (FMOs) for PMPR chromophore optimized at the B3LYP/6-311+G(d,p) level. For PMPR chromophore, the highest occupied molecular orbital (HOMO) and the lowest unoccupied molecular orbital (LUMO) are effectively delocalized and look quite similar in particular for the central styryl group. This indicates that they arise from significant electronic couplings between the fragment molecular orbitals of the central styryl group and neighboring substituents. We also note, however, that the HOMO and LUMO have more significant weights in the electron-donating piperidino and strong electron-withdrawing *N*-pyrimidinyl pyridinium groups, respectively, and thus are effectively separated. Such an orbital separation in PMPR chromophore is discerned clearer when the HOMO-1 and LUMO+1 states are compared. All these add up to a conclusion that the PMPR chromophore is a push-pull type π-conjugated chromophore and exhibits an efficient delocalization of π-electrons, which may result in large molecular optical nonlinearity.

PMPR cationic chromophore exhibits an extremely large maximum first hyperpolarizability β_{max} (OPT); 342 × 10^{-30} esu. The measured wavelength of maximum absorption λ_{max} for PMPR chromophore is also very high, 553 nm in methanol (Figure 3b),

which confirms the high molecular nonlinearity according to the general nonlinearity-transparency trade-off.[13] These values (β_{max} (OPT) and λ_{max}) are remarkably higher than the corresponding values for the chromophore DAS used in benchmark 4-(4-(dimethylamino)styryl)-1-methylpyridinium 4-methylbenzenesulfonate (DAST) crystals (β_{max} (OPT) = 159 × 10^{-30} esu and λ_{max} = 475 nm).[21] Moreover, they are also significantly higher than those of previously reported *N*-pyrimidinyl stilbazolium OPR chromophore having relatively weak electron-donating phenolic group (β_{max} (OPT) = 183 × 10^{-30} esu and λ_{max} = 443 nm).[17]

The molecular ordering angle θ_p, i.e., the angle between the direction of β_{max} and the symmetry *ac* crystallographic plane for PMPR-MO(I) crystals is very small; ~7 degree. This means that the molecular ordering of PMPR chromophores is close-to optimal for maximizing the macroscopic optical nonlinearity of PMPR-MO(I) crystals. The corresponding macroscopic optical nonlinearity is therefore extremely large for PMPR-MO(I) crystals. The diagonal component of the effective first hyperpolarizability $\beta_{iii}^{eff} = \beta_{max}(OPT) \cdot \cos^3\theta_p$ is 335 × 10^{-30} esu. This is about twice as large as in benchmark DAST crystals (161 × 10^{-30} esu).[21] Therefore, PMPR-MO(I) crystals with extremely large diagonal effective first hyperpolarizability β_{iii}^{eff} are very interesting materials for various nonlinear optical applications. In addition, PMPR-MO(I) crystals exhibit a high thermal stability up to ~ 260 °C as shown in Figure S4.

2.3. Efficient THz Wave Generation with Wide Flat-Spectral-Band

Large macroscopic second-order optical nonlinearity of organic crystals is highly beneficial to enhance the performance of diverse nonlinear optical devices. In THz wave generation, the optical-to-THz frequency conversion efficiency is proportional to the square of the macroscopic nonlinear optical coefficient of source materials.[9,10] Since PMPR-MO(I)

crystals possess a very large nonlinear optical coefficient ($\beta_{iii}^{\text{eff}} = 335 \times 10^{-30}$ esu), PMPR-MO(I) may act as an efficient THz wave generator with high conversion efficiency.

Figure 4a shows a photograph of an as-grown PMPR-MO(I) single crystal with an area of a few mm^2. This shows that PMPR-MO(I) has bulk crystal growth ability. Among organic crystals having large nonlinear optical coefficient, many crystals unfortunately exhibit poor growing ability for bulk crystals with a lateral size over mm-scale. Possessing bulk crystal growth ability for PMPR-MO(I) crystals is highly beneficial for real-world optical applications. The thickness of the as-grown PMPR-MO(I) single crystal is ultra-thin; about 10 μm and exhibit a strong optical anisotropy (Figure S5). The high anisotropy of PMPR-MO(I) single crystal originates from the parallel alignment of PMPR cations and MO anions (Figure 2a). Organic crystals both possessing an ultra-thin thickness and a large nonlinear optical coefficient show advantages for THz wave generation (i.e., dimple-free broad spectral bandwidth with high generation efficiency) as discussed below.

Using very thin THz source materials in the range from few μm to few tens of μm is a very attractive approach for achieving broadband THz wave generation. This is because an ultra-thin thickness can overcome the bandwidth limitations due to self-absorption and phase-mismatch between the used optical pump and the generated THz waves.[9,56] However, although very thin THz source materials can generate spectra with an ultra-broad bandwidth of THz waves, the resulting THz generation efficiency is in most cases very low compared to thicker crystals. This is because the generated THz amplitude is proportional to the thickness of THz source materials within the coherence length.[9] For example, widely used inorganic semiconducting THz source materials including GaAs, ZnTe, and GaP crystals were shown to generate broadband THz waves by using a very thin thickness, but with a very low THz conversion efficiency.[9] The conversion efficiency in this case is also limited by the macroscopic optical nonlinearity of inorganic semiconductors (e.g., about 4 pm/V for ZnTe), which is one order of magnitude

smaller than that of benchmark organic crystals. For thicker ZnTe crystals in the mm-scale (e.g., 1.0 mm), the bandwidth of the generated THz waves is limited with an upper cut-off generation frequency of less than 3 THz.[8] Consequently, as-grown PMPR-MO(I) single crystals having both an ultra-thin thickness and a large nonlinear optical coefficient are promising materials to generate THz waves with a broad, dimple-free spectrum and a high conversion efficiency.

To show the potential of PMPR-MO(I) crystals, THz wave generation experiments were performed with an ultra-thin PMPR-MO(I) single crystal having a thickness of 10 μm and the result was compared with that achieved in a 1.0-mm-thick ZnTe crystal. Near-infrared optical pulses at 1300 nm with a pulse duration of 140 fs at 1-kHz repetition rate were used as pump to generate THz waves in crystals by optical rectification. The pump beam diameter was about 0.5 mm at the average pump power of 10 mW. The generated THz waves were detected via electro-optic sampling in a 0.3-mm-thick GaP, where 800-nm pulses with 100-fs pulse duration were used to measure the THz electric field.

Figure 4b and 4c show the time traces and the corresponding spectra of the generated THz waves in PMPR-MO(I) and in reference ZnTe crystal. Although PMPR-MO(I) crystal have an ultra-thin thickness of about 10 μm, the generated THz amplitude is very high. Compared to the much thicker ZnTe crystal (1.0 mm), the peak-to-peak THz field generated in the 10-μm-thick PMPR-MO(I) crystal is 4.6 times higher. The results confirm that a very high optical-to-THz conversion efficiency could be achieved with PMPR-MO(I) crystal, which originates from its exceptionally large macroscopic optical nonlinearity. This high optical-to-THz conversion efficiency of only a 10-μm thick PMPR-MO(I) crystal is outstanding; many organic benchmark THz-generation crystals with the thickness of few hundred micrometers generate about one order of magnitude higher THz electric-field than ZnTe (1.0 mm) at very similar experimental conditions with this work.[9]

Furthermore, the THz waves generated in PMPR-MO(I) crystal show a very flat, dimple-free broadband spectrum. As shown in Figure 4c, the generated THz waves exhibit an extremely broad flat spectral band in the frequency range of 0.7-3.4 THz. The flat-spectral-band in the present work is defined as the frequency range, for which the difference between the highest and the lowest THz amplitude is below 3 dB. Note that this is comparable or even better than the preferred spectral bandwidth, shape and extinction ratio of conventional band-pass filters. As illustrated in Scheme 1c, an ideal spectroscopic source should provide as broad and as flat spectral band as possible for application in broadband (THz) spectroscopy.

In addition, the entire THz spectrum from PMPR-MO(I) crystal does not show strong dimples. In most organic THz generators, many dimples usually appeared as illustrated in Scheme 1d. Moreover, the total useful bandwidth of the generated THz spectrum from PMPR-MO(I) crystal is extremely broad at the pump pulse duration of 140 fs. The upper cut-off generation frequency is ~7 THz as shown in Figure S6. Figure S7 shows the measured absorbance of a PMPR-MO(I) single crystal along the polar axis in THz frequency range. The absorbance of as-grown ultra-thin 10-μm-thick PMPR-MO(I) crystal is very small; only very broad and small peaks at 2.0 and 4.5 THz were observed. In many benchmark organic THz generators with the thickness over hundred micrometers, the self-absorption in the THz frequency range due to phonon/vibrational modes was shown to limit the generated THz spectral bandwidth and cause undesired spectral dimples.[9,56] However, with ultra-thin organic crystals (10 μm as in this work), the influence of self-absorption on THz-wave generation characteristics may be negligible because of a relatively very small absorption (Figure S7). Note that even in much thicker benchmark organic THz-generation crystals with a thickness of 100 μm, the reduction of the generated THz spectrum by self-absorption was already reported to be very small.[56] Ultra-thin thickness of PMPR-MO(I) single crystals is therefore highly beneficial to obtain a very flat and broadband THz generation spectrum without strong dimples. Consequently, PMPR-MO(I) single crystal with an ultra-thin thickness of 10 μm and the

extremely large diagonal component of the effective first hyperpolarizability β_{iii}^{eff} enabled us to simultaneous achieve i) a well-defined dimple-free flat THz spectrum and ii) a high optical-to-THz frequency conversion efficiency.

2.4. Crystal Characteristics

For practical applications including THz-wave generation, other crystal characteristics beyond the large macroscopic optical nonlinearity are important. Figure S8 shows the result of a hygroscopy test of PMPR-MO(I) crystal on a water droplet. PMPR-MO(I) crystals show high water resistance; i.e., a high environmental stability against humidity. Note that many organic nonlinear optical salt crystals are highly soluble in water and may even exhibit a phase transition to a hydrated phase (DAST for example).

In addition, obtaining ultra-thin thickness (e.g., 10 μm as shown in Figure S5) of as-grown PMPR-MO(I) single crystals is highly beneficial. Note that the growth of ultra-thin organic nonlinear optical single crystals with few micrometers to few tens of micrometers is very difficult and usually required special crystal growth techniques.[32,57,58] Moreover, simultaneous achievement of a relative large area over few mm^2 scale is also very interesting for various (nonlinear optical) photonic applications.[1,3,9,32,59,60] The thin plate morphology of as-grown PMPR-MO(I) single crystals is suitable for diverse optical experiments without additional polishing and cutting processes, as used in our THz generation experiments. Consequently, PMPR-MO(I) single crystals having extremely large diagonal optical nonlinearity exhibit high environmental stability and good crystal growing ability resulting in ultra-thin single crystals with the area of over few mm^2.

3. Conclusion

In summary, we have newly developed highly efficient second-order nonlinear optical organic crystals based on *N*-pyrimidinyl stilbazolium PMPR chromophores possessing

extremely large maximum first hyperpolarizability β_{max} of 342 × 10^{-30} esu. Incorporating a highly nonlinear PMPR cationic chromophore, a head-to-tail cation-anion O-H···O hydrogen-bonding synthon, and an optimal selection of the counter anion with an appropriate size result in extremely large macroscopic optical nonlinearity with the effective first hyperpolarizability β_{iii}^{eff} of 335 × 10^{-30} esu. To the best of our knowledge, this is the first report of organic crystals having such an extremely large effective first hyperpolarizability β_{iii}^{eff} > 300 × 10^{-30} esu and a bulk crystal growth ability . Based on this extremely large macroscopic optical nonlinearity and an ultra-thin thickness, PMPR-MO single crystal allows us to generate dimple-free broadband THz waves with a wide flat-spectral-band in the range of 0.7-3.4 THz at -3dB, a large upper cut-off frequency of > 7 THz and a high generation efficiency. Therefore, new class of organic nonlinear optical PMPR-MO crystals are very interesting materials for practical nonlinear optical applications. In addition, the design approach we applied for PMPR-MO crystals (incorporating cation-anion O-H···O hydrogen-bonding synthon and anion selection with an optimal size) may be very beneficial for designing further highly efficient organic crystals based on chromophores possessing extremely large molecular optical nonlinearity.

4. Experimental Section

The details of synthesis, crystallization process, X-ray crystal structure analysis, powder SHG measurements, optical nonlinearity, thermal stability, crystal morphology, and THz wave generation are described in the Supporting Information (SI).

Supporting Information

Supporting Information is available from the Wiley Online Library or from the author.

Acknowledgements

S. J. K and I. C. Y. contributed equally to this work. This work has been supported by the National Research Foundation of Korea (NRF) funded by the Ministry of Science, ICT & Future Planning, Korea (No. 2021R1A2C1005012, 2021R1A5A6002853,

2019K1A3A1A14057973, 2019R1A2C3003504), Institute of Information & communications Technology Planning & Evaluation (IITP) grant funded by the Korea government (MSIT) (No. 2022-0-00624) and Swiss National Science Foundation (SNSF), Switzerland (No. IZKSZ2_188194). X-ray structural analysis was supported by Basic Science Research Program through the National Research Foundation of Korea(NRF) funded by the Ministry of Education (2019R1I1A2A01058066).

Received: ((will be filled in by the editorial staff))
Revised: ((will be filled in by the editorial staff))
Published online: ((will be filled in by the editorial staff))

References

[1] Q. Ma, A. G. Grushin, K. S. Burch, *Nat. Mater.* **2021**, *20*, 1601.

[2] H. Xu, D. L. Elder, L. E. Johnson, Y. De Coene, S. R. Hammond, W. V. Ghinst, K. Clays, L. R. Dalton, B. H. Robinson, *Adv. Mater.* **2021**, *33*, 2104174.

[3] G. Lu, J. Hong, F. Qiu, A. M. Spring, T. Kashino, J. Oshima, M. Ozawa, H. Nawata, S. Yokoyama, *Nat. Commun.* **2020**, *11*, 4224.

[4] Y.Enami, C. T. Derose, D. Mathine, C. Loychik, C. Greenlee, R. A. Norwood, T. D. Kim, J. Luo, Y. Tian, A. K. -Y. Jen, N. Peyghambarian, *Nat. Photonics* **2007**, *1*, 180.

[5] L. Chang, S. Liu, J. E. Bowers, *Nat. Photonics* **2022**, *16*, 95.

[6] B. Zhang, L. Wang, F. Chen, *Laser Photonics Rev.*, **2020**, *14*, 1900407

[7] M. Annadhasan, S. Basak, N. Chandrasekhar, R. Chandrasekar, *Adv. Opt. Mater.* **2020**, *8*, 2000959.

[8] J. A. Fülöp, S. Tzortzakis, T. Kampfrath, *Adv. Opt. Mater*. **2020**, *8*, 1900681.

[9] S. J. Kim, B. J. Kang, U. Puc, W. T. Kim, M. Jazbinsek, F. Rotermund, O. P. Kwon, *Adv. Opt. Mater.* **2021**, *9*, 2101019.

[10] J. Hebling, K.L. Yeh, M. C. Hoffmann, B. Bartal, K. A. Nelson, *J. Opt. Soc. Am. B*. **2008**, *25*, B6.

[11] M. Martin, J. Mangeney, P. Crozat, P. Mounaix, *Appl. Phys. Lett*. **2010,** *97*, 111112.

[12] A. Schneider, I. Biaggio, P. Günter, *Appl. Phys. Lett*. **2004,** *84*, 2229.

[12] O. P. Kwon, S. J. Kwon, M. Jazbinsek, F. D. J. Brunner, J. I. Seo, Ch. Hunziker, A. Schneider, H. Yun, Y. S. Lee, P. Günter, *Adv. Funct. Mater.* **2008**, *18*, 3242.

[13] Ch. Bosshard, M. Bösch, I. Liakatas, M. Jäger, P. Günter, in *Nonlinear Optical Effects and Materials* (Ed: P. Günter), Springer-Verlag, Berlin **2000**, Ch. 3.

[14] L. R. Dalton, P. A. Sullivan, D. H. Bale, *Chem. Rev*. **2010**, *110*, 25.

[15] B. J. Coe, J. A. Harris, I. Asselberghs, K. Clays, G. Olbrechts, A. Persoons, J. T. Hupp, R. C. Johnson, S. J. Coles, M. B. Hursthouse, K. Nakatani, *Adv. Funct. Mater*. **2002**, *12*, 110.

[16] B. R. Shin, S. I. Kim, D. W. Kim, M. Jazbinsek, W. J. Yoon, H. S. Yun, I. C. Yu, F. Rotermund, O. P. Kwon, *Opt. Laser Technol.,* **2022**, 108454.

[17] S. J. Kim, S. I. Kim, M. Jazbinsek, W. J. Yoon, H. S. Yun, D. W. Kim, I. C. Yu, F. Rotermund, O. P. Kwon, *Adv. Photonics Res.* **2022**, 3, 2100350.

[18] B. J. Coe, J. A. Harris, I. Asselberghs, K. Clays, G. Olbrechts, A. Persoons, J. T. Hupp, R. C. Johnson, S. J. Coles, M. B. Hursthouse, K. Nakatani, *Adv. Funct. Mater*. **2002**, *12*, 110.

[19] B. J. Coe, D. Beljonne, H. Vogel, J. Garin, J. Orduna, *J. Phys. Chem. A* **2005**, *109*, 10052.

[20] S. R. Marder, J. W. Perry, W. P. Schaefer, *Science* **1989**, *245*, 626.

[21] P. J. Kim, J. H. Jeong, M. Jazbinsek, S. J. Kwon, H. Yun, J. Kim, Y. S. Lee, I. H. Baek, F. Rotermund, P. Günter, O. P. Kwon*, CrystEngComm* **2011**, *13*, 444.

[22] J. H. Seok, D. J. Kim, W. T. Kim, S. J. Kim, W. J. Yoon, G. E. Yoon, I. C. Yu, M. Jazbinsek, S. W. Kim, H. S .Yun, D. W. Kim, F. Rotermund, O. P. Kwon, *Adv. Opt. Mater.* **2021**, *9*, 2100324.

[23] S. C. Lee, B. J. Kang, J. A. Lee, S. H. Lee, M. Jazbinšek, W. Yoon, H. Yun, F. Rotermund, O. P. Kwon, *Adv. Opt. Mater*. **2018**, *6*, 1701258.

[24] J. A. Lee, W. T. Kim, M. Jazbinsek, D. Kim, S. H. Lee, S. H. Lee, I. C. Yu, W. Yoon, H. Yun, F. Rotermund, O. P. Kwon, *Adv. Opt. Mater*. **2020**, *8*, 1901921.

[25] G. A. Valdivia-Berroeta, E. W. Jackson, K. C. Kenney, A. X. Wayment, I. C. Tangen, C. B. Bahr, S. J. Smith, D. J. Michaelis, J. A. Johnson, *Adv. Funct. Mater*. **2020**, *30*, 1904786.

[26] I. Aramburu, J. Ortega, C. L. Folcia, J. Etxebarria, *Appl. Phys. Lett.* **2014**, *104*, 071107.

[27] S. K. Kurtz, T. T. Perry, *J. Appl. Phys.* **1968**, *39*, 3798.

[28] C. U. Jeong, B. J. Kang, S. H. Lee, S. C. Lee, W. T. Kim, M. Jazbinsek, W. Yoon, H. Yun, D. Kim, F. Rotermund, O. P. Kwon, *Adv. Funct. Mater*. **2018**, *28*, 1801143.

[29] J. H. Seok, U. Puc, S. J. Kim, W. J. Yoon, H. S. Yun, I. C. Yu, F. Rotermund, D. W. Kim, M. Jazbinsek, O. P. Kwon, *Adv. Opt. Mater*. **2021**, *9*, 2100618

[30] G. E. Yoon, J. H. Seok, U. Puc, B. R. Shin, W. J. Yoon, H. S. Yun, D. W. Kim, I. C. Yu, F. Rotermund, M. Jazbinsek, O. P. Kwon, *Adv. Sci.* **2022**, 2201391.

[31] A. Sher Gill, S. Kalainathan, *J. Phys. Chem. Solids*, **2011**, *72*, 1002.

[32] Z. Yang, L. Mutter, M. Stillhart, B. Ruiz, S. Aravazhi, M. Jazbinsek, A. Schneider, V. Gramlich, P. Günter, *Adv. Funct. Mater.* **2007***, 17*, 2018.

[33] B. Ruiz, Z. Yang, V. Gramlich, M. Jazbinsek, P. Günter, *J. Mater. Chem*, **2006**, *16*, 2839.

[34] Z. Sun, X. Liu, X. Wang, L. Li, X. Shi, S. Li, C. Ji, J. Luo, M. Hong, *Cryst. Growth Des.* **2012**, *12*, 6181.

[35] G. A. Valdivia-Berroeta, L. K. Heki, E. A. McMurray, L. A. Foote, S. H. Nazari, L. Y. Serafin, S. J. Smith, D. J. Michaelis, J. A. Johnson, *Adv. Opt. Mater*. **2018**, *6*, 1800383.

[36] G. A. Valdivia-Berroeta, K. C. Kenney, E. W. Jackson, J. C. Bloxham, A. X. Wayment, D. J. Brock, S. J. Smith, J. A. Johnson, D. J. Michaelis*, J. Mater. Chem. C* **2020**, *8*, 11079.

[37] P. J. Kim, J. H. Jeong, M. Jazbinsek, S. B. Choi, I. H. Baek, J. T. Kim, F. Rotermund, H. Yun, Y. S. Lee, P. Günter, O. P. Kwon, *Adv. Funct. Mater.* **2012**, *22*, 200.

[38] J. H. Jeong, B. J. Kang, J. S. Kim, M. Jazbinsek, S. H. Lee, S. C. Lee, I. H. Baek, H. Yun, J. Kim, Y. S. Lee, J. H. Lee, J. H. Kim, F. Rotermund, O. P. Kwon, *Sci. Rep*. **2013**, *3*, 3200.

[39] S. H. Lee, B. J. Kang, B. W. Yoo, S. C. Lee, S. J. Lee, M. Jazbinsek, H. Yun, F. Rotermund, O. P. Kwon, *Adv. Funct. Mater*. **2017**, *27*, 1605583.

[40] S. I. Kim, B. J. Kang, C. U. Jeong, M. H. Shin, W. T. Kim, M. Jazbinsek, W. Yoon, H. Yun, D. Kim, F. Rotermund, O. P. Kwon, *Adv. Opt. Mater*. **2019**, *7*, 1801495.

[41] S. I. Kim, W. T. Kim, J. H. Seok, M. Jazbinsek, W. Yoon, I. C. Yu, H. Yun, D. Kim, F. Rotermund, O. P. Kwon, *Adv. Opt. Mater*. **2020**, *8*, 1901840.

[42] S. H. Lee, B. J. Kang, J. S. Kim, B. W. Yoo, J. H. Jeong, K. H. Lee, M. Jazbinsek, J. W. Kim, H. Yun, J. Kim, Y. S. Lee, F. Rotermund, O. P. Kwon, *Adv. Opt. Mater*. **2015**, *3*, 756.

[43] S. J. Lee, B. J. Kang, M. H. Shin, S. C. Lee, S. H. Lee, M. Jazbinsek, H. Yun, D. Kim, F. Rotermund, O. P. Kwon, *Adv. Opt. Mater*. **2018**, *6*, 1700930.

[44] S. C. Lee, B. J. Kang, M. J. Koo, S. H. Lee, J. H. Han, J. Y. Choi, W. T. Kim, M. Jazbinsek, H. Yun, D. Kim, F. Rotermund, O. P. Kwon, *Adv. Opt. Mater*. **2017**, *5*, 1600758.

[45] M. H. Shin, W. T. Kim, S. I. Kim, S. H. Lee, I. C. Yu, M. Jazbinsek, W. Yoon, H. Yun, D. Kim, F. Rotermund, O. P. Kwon, *Adv. Opt. Mater*. **2019**, *7*, 1900953.

[46] J. Y. Choi, S. J. Lee, S. C. Lee, C. U. Jeong, M. Jazbinsek, H. Yun, B. J. Kang, F. Rotermund, O. P. Kwon, *J. Mater. Chem. C*, **2017**, *5*, 12602

[47] S. H. Lee, J. Lu, S. J. Lee, J. H. Han, C. U. Jeong, S. C. Lee, X. Li, M. Jazbinsek, W. Yoon, H. Yun, B. J. Kang, F. Rotermund, K. A. Nelson, O. P. Kwon, *Adv. Mater*. **2017**, *29*, 1701748.

[48] M. H. Shin, W. T. Kim, S. I. Kim, S. J. Kim, I. C. Yu, S. W. Kim, M. Jazbinsek, W. Yoon, H. Yun, F. Rotermund, O. P. Kwon, *Adv. Sci*. **2020**, *7*, 2001738.

[49] D. Kim, W. T. Kim, J. H. Han, J. A. Lee, S. H. Lee, B. J. Kang, M. Jazbinsek, W. Yoon, H. Yun, D. Kim, S. Bezouw, J. Campo, W. Wenseleers, F. Rotermund, O. P. Kwon, *Adv. Opt. Mater.* **2020**, *8*, 1902099.

[50] J. Shi, Y. He, F. Liang, X. Zhang, D. Xu, J. Yao, G. Zhang, Z. Hu, J. Yao, Y. Wu, *J. Mater. Chem. C* **2020**, *8*, 4226.

[51] D. Kim, W. T. Kim, J. H. Seok, I. C. Yu, M. Jazbinsek, W. Yoon, H. Yun, D. Kim, F. Rotermund, O. P. Kwon, *J. Mater. Chem. C* **2020**, *8*, 10078.

[52] M. A. Spackman, J. J. McKinnon, *CrystEngComm* **2002,** *4*, 378

[53] M. A. Spackman, D. Jayatilaka, *CrystEngComm* **2009**, *11*, 19.

[54] J. J. McKinnon, D. Jayatilaka, M. A. Spackman, *Chem. Commun.* **2007**, *37*, 3814

[55] S. H. Lee, M. Jazbinsek, C. P. Hauri, O. P. Kwon, *CrystEngComm* **2016**, *18*, 7180.

[56] J. Kim, Y. C. Park, J. H. Seok, M. Jazbinsek, O. P. Kwon, *Adv. Opt. Mater*. **2021**, *9*, 2001521.

[57] O. P. Kwon, S. J. Kwon, H. Figi, M. Jazbinsek, P. Gunter, *Adv. Mater*., **2008**, *20,* 543.

[58] A. Choubey, O. P. Kwon, M. Jazbinsek, P. Gunter, *Cryst. Growth Des*. **2007**, *7*, 402.

[59] J. Shi, F. Liang, Y. He, X. Zhang, Z. Lin, D. Xu, Z. Hu, J. Yao, Y. Wu, *Chem. Commun*. **2019**, *55*, 7950.

[60] W. Zhang, Z. Wang, X. Zhang, Y. Wang, D. Xu, Z. Hu, J. Yao, Y. Wu, *Cryst. Growth Des*. **2022**, *22*, 3311.

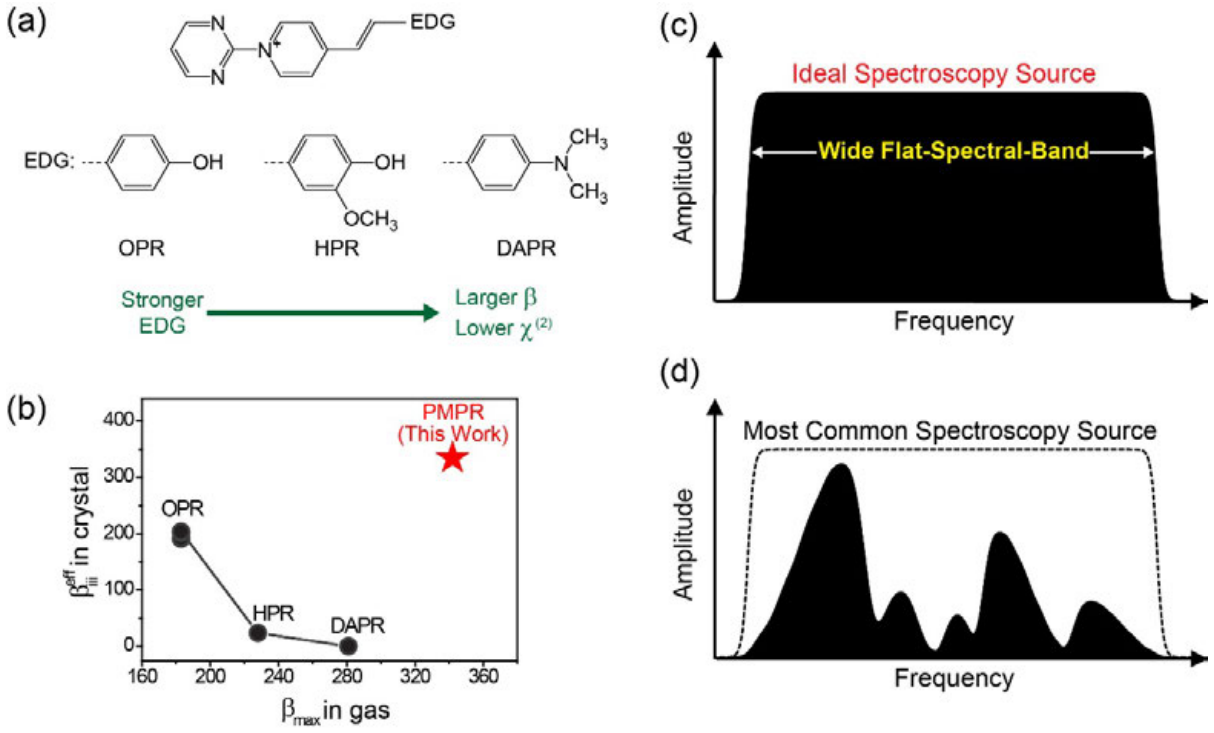

Scheme 1. (a) Previously reported *N*-pyrimidinyl stilbazolium chromophores (OPR, HPR, and DAPR) with various electron donating groups (EDGs) and (b) their molecular optical nonlinearity (maximum first hyperpolarizability β_{max} in gas phase) and macroscopic optical nonlinearity (effective first hyperpolarizability β_{iii}^{eff} in crystals).[15-17] For comparison, newly designed PMPR chromophore in this work is also presented. Schematic of (c) ideal spectroscopy source with wide flat-spectral-band and (d) most common source with absorption dimples for broadband THz spectroscopy.

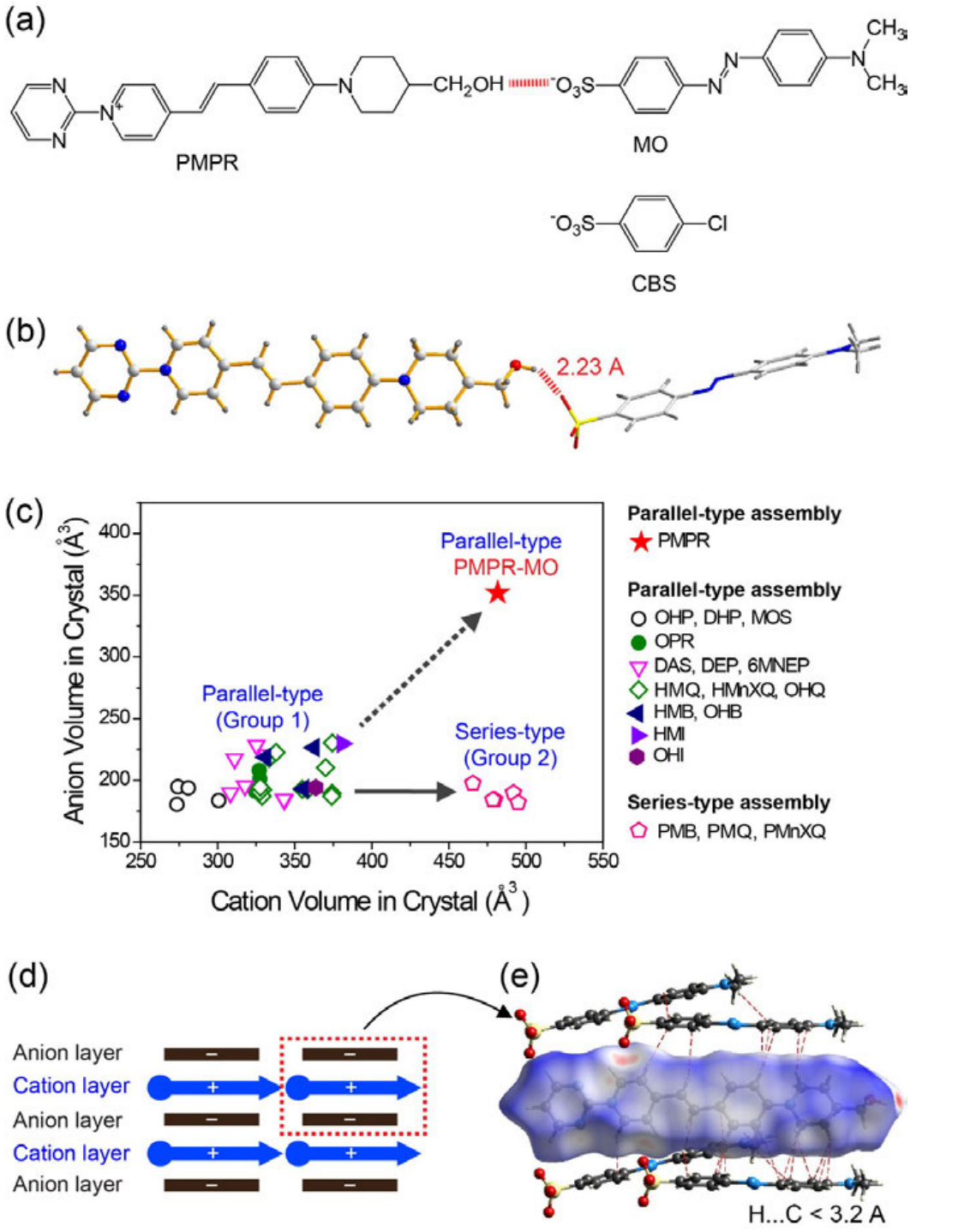

Figure 1. (a) Newly designed PMPR-MO and PMPR-CBS. (b) Head-to-tail cation-anion assembly based on strong hydrogen bond between -OH···$^{-}$O$_3$S- groups in PMPR-MO(I) crystals. (c) Crystallographic volume of molecular cations and anions in benchmark organic nonlinear optical crystals, determined from Hirshfeld surface analysis. (d) Schematic of parallel-type assembly in benchmark organic salt crystals. (e) Hirshfeld surface of PMPR cation, presenting X···Y close contacts of H···C (≤ 3.2 Å, red dotted lines), in PMPR-MO(I) crystals.

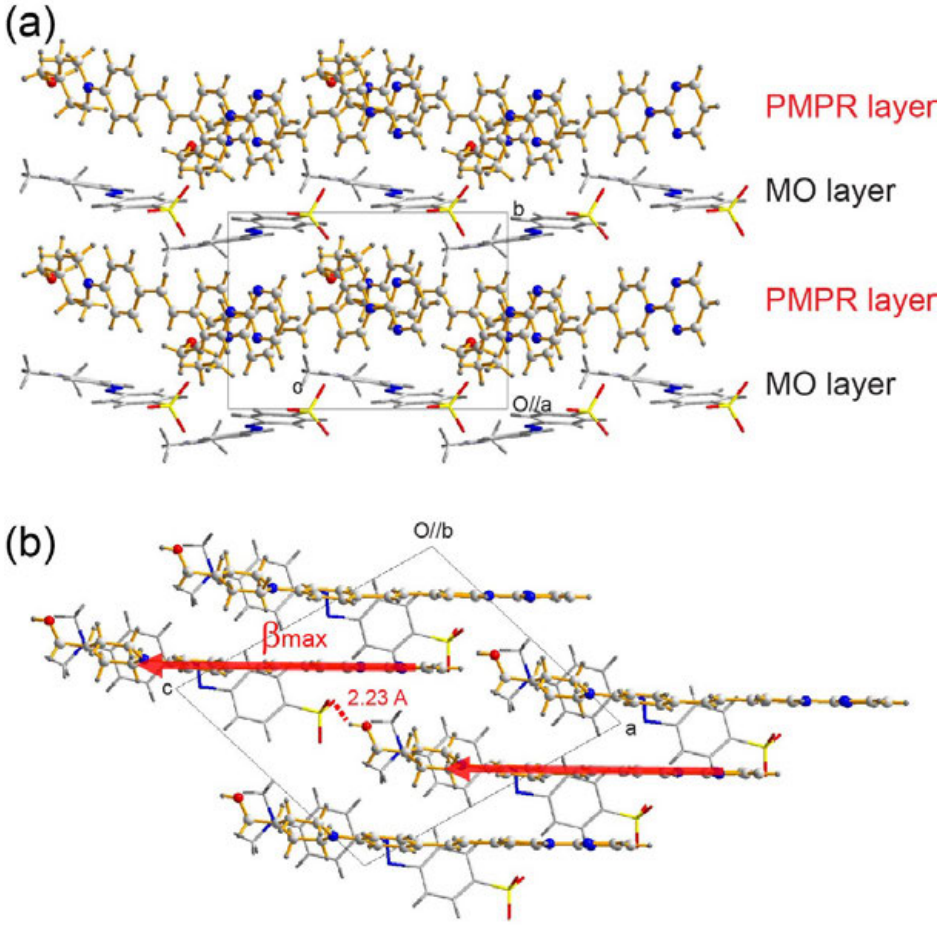

Figure 2. Molecular ordering of PMPR-MO (I) crystals with monoclinic *P*c space group. The solid arrows present the direction of the first hyperpolarizability β_{max} of PMPR cations.

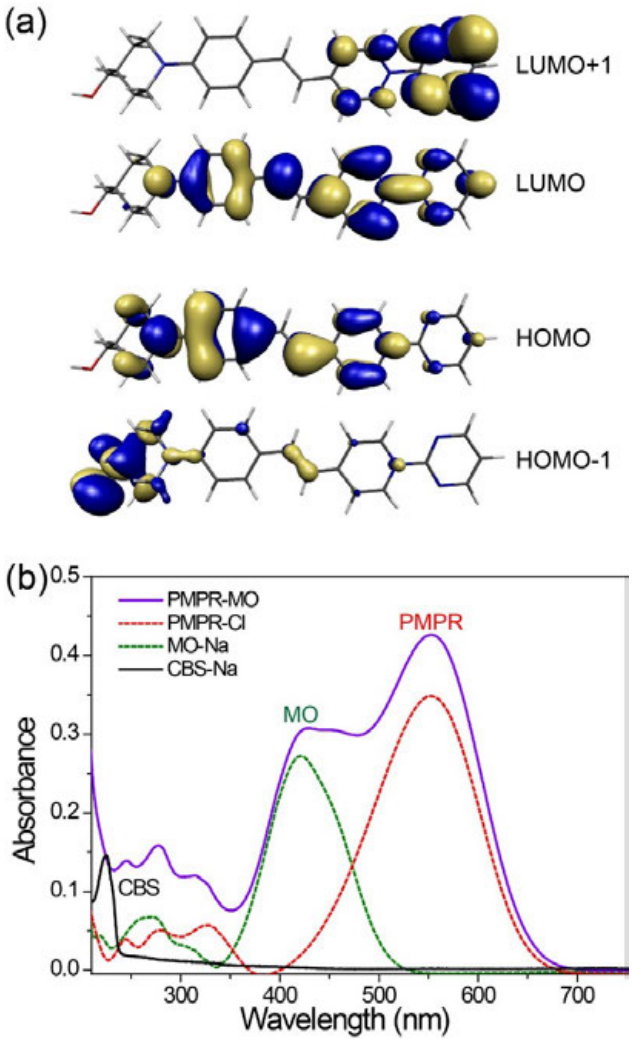

Figure 3. (a) Frontier molecular orbital pairs at B3LYP/6-311+g(d,p) for PMPR chromophore. (b) Absorption spectra of PMPR-MO, PMPR-Cl, MO-Na, and CBS-Na in methanol (10^{-5} *M*).

.

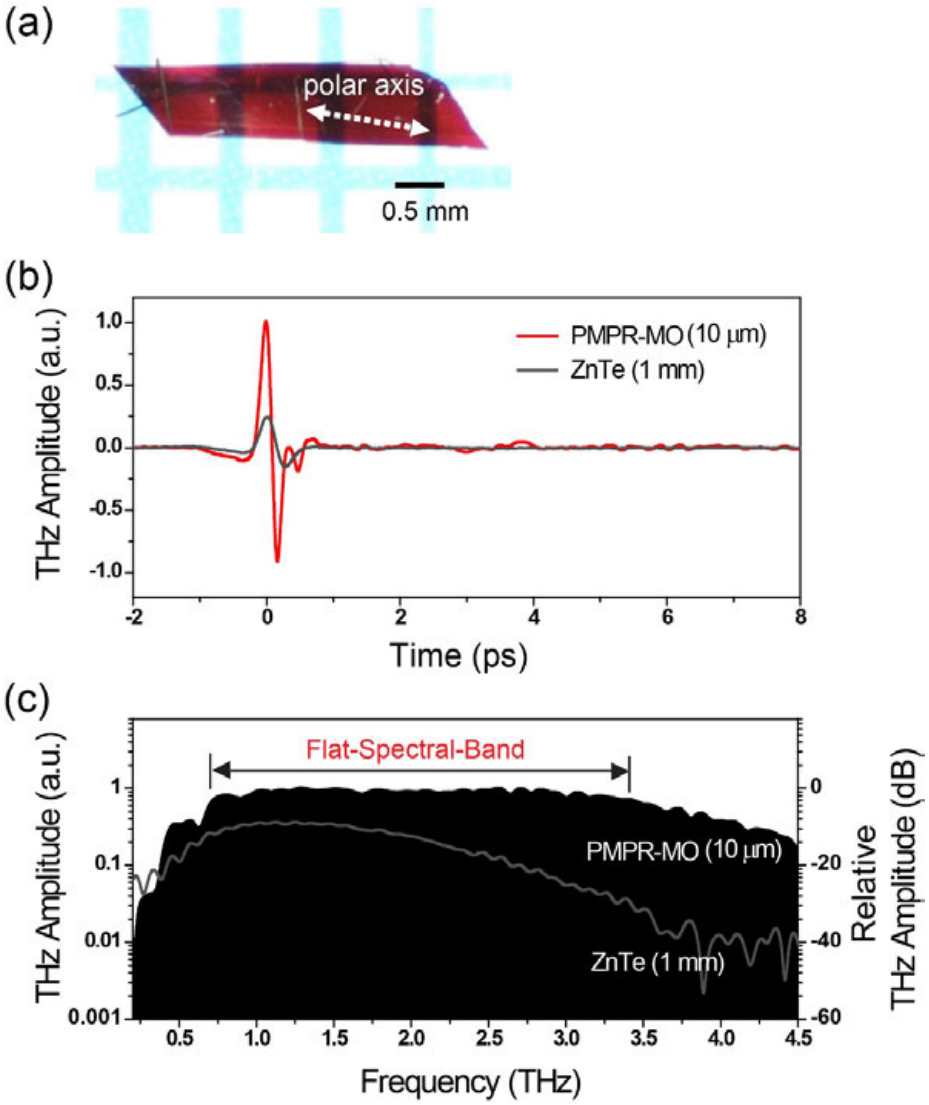

Figure 4. (a) Ultra-thin PMPR-MO(I) crystal with a thickness of ~10 μm (see Figure S5 for the side view). THz generation in 10 μm-thick PMPR-MO(I) and 1.0 mm-thick ZnTe crystals, pumped at 1300 nm: (b) time traces and (c) the corresponding generated spectra, for which full spectra up to 8 THz are shown in Figure S6. The THz amplitude is normalized to 1.0 for the highest THz amplitude of PMPR-MO(I). The flat-spectral-band is here defined between the highest and lowest THz frequencies at -3dB of the highest THz amplitude.

Table of Contents

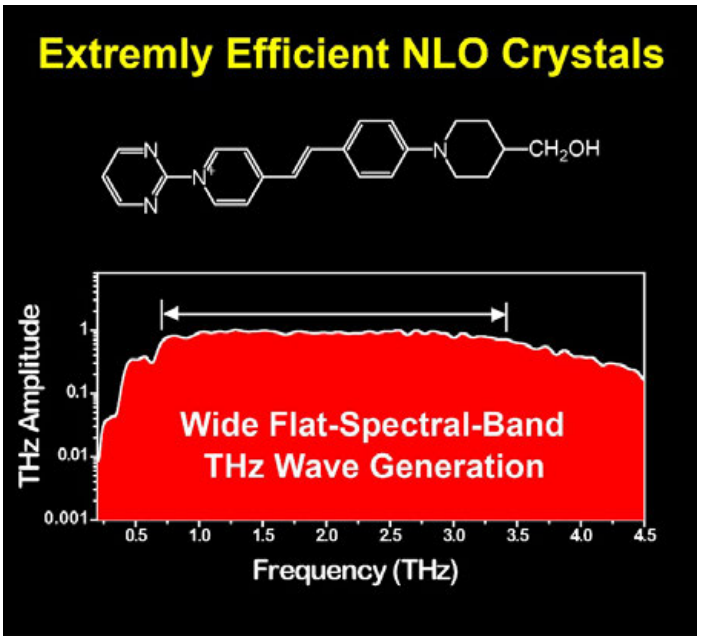

Newly designed 4-(4-(4-(hydroxymethyl)piperidin-1-yl)styryl)-1-(pyrimidin-2-yl)pyridin-1-ium (PMPR) crystals possessing extremely large macroscopic optical nonlinearity (335×10^{-30} esu) exhibit broadband THz wave generation with a wide flat-spectral-band in the range of 0.7-3.4 THz together with a high generation efficiency.

Supporting Information

A New Class of Organic Crystals with Extremely Large Hyperpolarizability: Efficient THz Wave Generation with Wide Flat-Spectral-Band

Seung-Jun Kim†, In Cheol Yu†, Dong-Joo Kim, Mojca Jazbinsek, Woojin Yoon, Hoseop Yun, Dongwook Kim, Fabian Rotermund, O-Pil Kwon**

((Optional Dedication))

S. J. Kim, D. J. Kim, Prof. O. P. Kwon
Department of Molecular Science and Technology, Ajou University, Suwon 16499 (Korea)
E-mail: opilkwon@ajou.ac.kr
I. C. Yu, Prof. F. Rotermund
Department of Physics, Korea Advanced Institute of Science and Technology (KAIST), Daejeon 34141 (Korea)
E-mail: rotermund@kaist.ac.kr
Dr. M. Jazbinsek
Institute of Computational Physics, Zurich University of Applied Sciences (ZHAW), 8401 Winterthur (Switzerland)
W. Yoon, Prof. H. Yun
Department of Chemistry & Department of Energy Systems Research, Ajou University, Suwon 16499 (Korea)
Prof. D. Kim
Department of Chemistry, Kyonggi University, San 94-6, Iui-dong, Yeongtong-gu, Suwonsi, Gyeonggi 443-760 (Korea)

†These authors equally contributed to this work.

A. Summary of Synthesis and Crystallization Processes for PMPR-MO

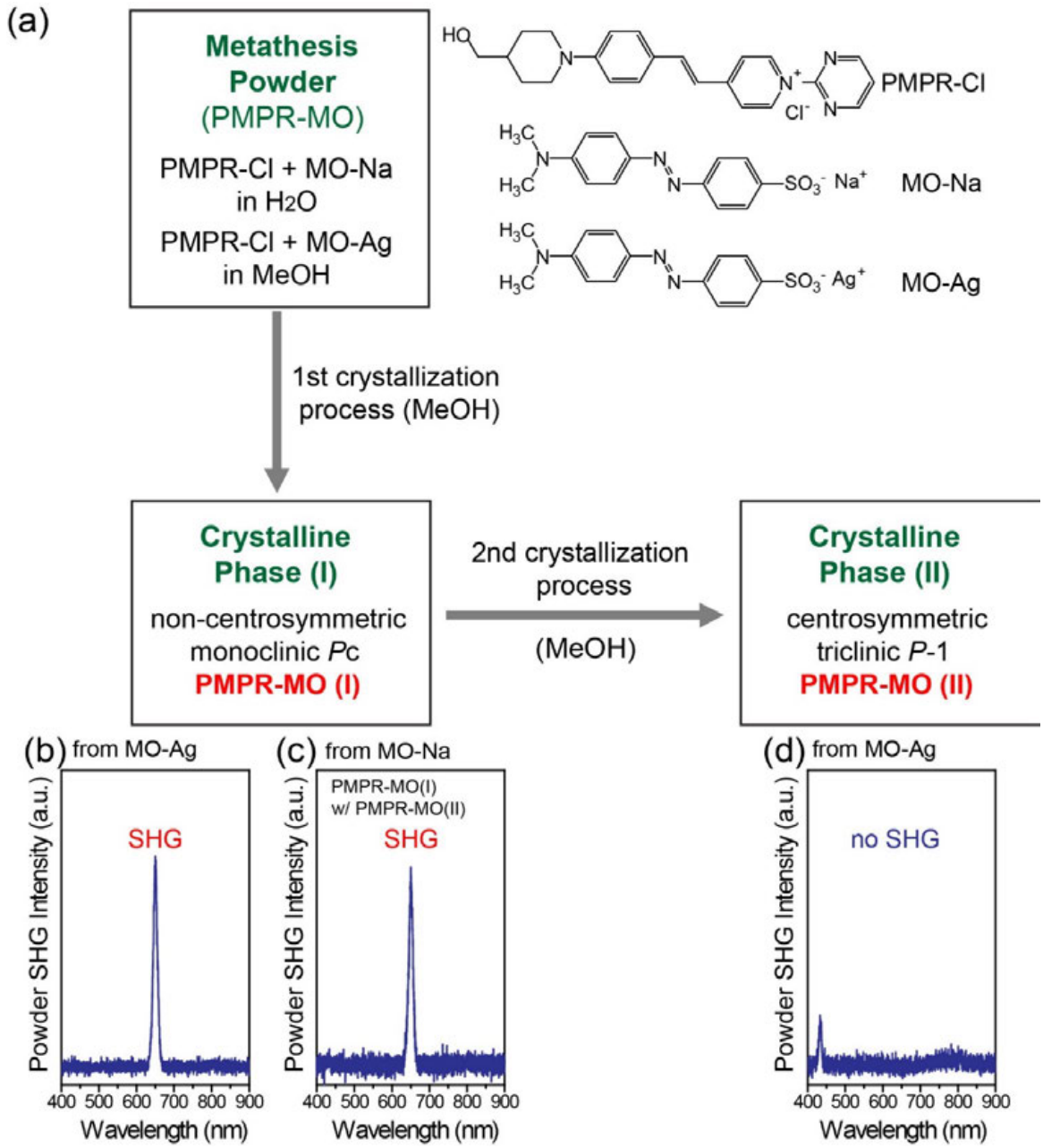

Figure S1. (a) Synthesis and crystallization processes of PMPR-MO crystals used in this work. The details of the synthesis and X-ray single crystal structure analysis are described in Section B and C, respectively. (b-d) Powder second harmonic generation (SHG) experiments of the crystalline phase-I and -II at the fundamental pump wavelength of 1300 nm.

The so-called metathesis powders of PMPR-MO in Figure S1a were obtained by a precipitation method from the PMPR-Cl and MO-Na in water solution (or MO-Ag in methanol solution). All crystallization processes used in this work are based on solution-cooling method in methanol. In both the first and the second crystallization processes, various crystallization conditions (e.g., cooling rate and saturation temperature) were examined.

In the first crystallization process of metathesis powders, the crystalline phase I of PMPR-MO with non-centrosymmetric monoclinic *Pc* space group (the crystal structure of CCDC-2101311) always formed at our experimental conditions. All crystalline powders obtained from the first crystallization process, based on both MO-Na and MO-Ag, exhibited a strong SHG signal (Figure S1b and S1c). In this work, the PMPR-MO crystals with non-centrosymmetric monoclinic *Pc* space group are denoted as PMPR-MO(I) crystals.

In contrast, in the second crystallization process, the crystalline phase II of PMPR-MO with centrosymmetric triclinic *P*-1 space group (e.g., the crystal structure of CCDC-2070574) always formed. As shown in Figure S1d, no SHG signals were observed. The centrosymmetric PMPR-MO crystals with triclinic *P*-1 space group are denoted as PMPR-MO (II) crystals.

Note that in the first crystallization process, concomitant polymorphism was observed. In an experimental condition of the first crystallization process (Figure S1c), we observed the concomitant formation of polymorphs. In the same crystal growth batch, centrosymmetric PMPR-MO(II) single crystals (CCDC-2101310 with only minor differences to CCDC-2070574, see Section C and Figure S2) were grown along with non-centrosymmetric PMPR-MO(I) single crystals (CCDC-2101311). When different crystallization conditions were used, PMPR-MO(I) crystals (and bulk single crystals) can be grown. Although we observed concomitant polymorphism of PMPR-MO crystals, it is obvious that non-centrosymmetric PMPR-MO(I) single crystals with a high potential for diverse nonlinear optical applications can be grown in the first crystallization process.

B. Synthesis

4-(4-(4-(Hydroxymethyl)piperidin-1-yl)styryl)-1-(pyrimidin-2-yl)pyridin-1-ium chloride (PMPR-Cl): 4-(4-(Hydroxymethyl)piperdin-1-ylbenzaldehyde (3.5 g, 16 mmol) and 4-methyl-1-(pyrimidin-2-yl)pyridin-1-ium chloride (3.3 g, 16 mmol) were dissolved in methanol (120 mL) and then piperidine was added (0.27 g, 3.2 mmol). The solution was stirred at 50 °C for 17 h. After cooling to room temperature, powder was obtained by precipitation in ethyl acetate and then dried in vacuum oven at 105 °C for ~6 h. Yield 33%. ^{1}H-NMR (600 MHz, DMSO-d_6, δ): 9.64 (d, 2H, J = 7.6 Hz, $C_5H_4N^+$), 9.17 (d, 2H, J = 4.8 Hz, $C_4H_3N_2$), 8.18 (d, 2H, J = 7.2 Hz, $C_5H_4N^+$), 8.17 (d, 1H, J = 14.4 Hz, C_2H_2), 7.88 (t, 1H, J = 4.8 Hz, $C_4H_3N_2$), 7.70 (d, 2H, J = 9.0 Hz, C_6H_4), 7.40 (d, 1H, J = 15.8 Hz, C_2H_2), 7.05 (d, 2H, J = 9.0 Hz, C_6H_4), 4.52 (s, 1H, CH_3O), 4.03 (d, 2H, J = 13.1 Hz, CH_3O), 3.28 (d, 2H, J = 5.5Hz, C_5H_9N), 2.90 (t, 2H, J = 12.9 Hz, C_5H_9N), 1.75 (d, 2H, J = 12.4 Hz, C_5H_9N), 1.65 (m, 1H, C_5H_9N), 1.19 (m, 2H, C_5H_9N).

4-(4-(4-(Hydroxymethyl)piperidin-1-yl)styryl)-1-(pyrimidin-2-yl)pyridin-1-ium 4-((4-(dimethylamino)phenyl)diazenyl)benzenesulfonate (PMPR-MO) from MO-Na: PMPR-Cl (0.6 g, 1.47 mmol) was dissolved in water (500 mL) at 55°C and sodium 4-((4-(dimethylamino)phenyl)diazenyl)benzenesulfonate (MO-Na, 0.5 g, 1.47 mmol) was dissolved in water (100 mL). Two solutions were mixed and stirred at 55°C for 30 min. When two solutions were mixed, powder was immediately precipitated. After cooling to room temperature, the solution was kept for 14 h. The precipitated powder was obtained by filtration (metathesis powder in Figure S1a). In the first crystallization process (recrystallization in methanol), the crystalline powder was obtained and dried in vacuum oven at 105 ºC for ~15 h (crystalline Phase-I in Figure S1a). Yield = 62%. ^{1}H-NMR (600 MHz, DMSO-d_6, δ) : 9.64 (d, 2H, J = 6.6 Hz, $C_5H_4N^+$), 9.16 (d, 2H, J = 4.8 Hz, $C_4H_3N_2$), 8.18 (d, 2H, J = 7.8 Hz, $C_5H_4N^+$), 8.16 (d, 1H, J = 15.6 Hz, C_2H_2), 7.87 (t, 1H, J = 4.8 Hz, $C_4H_3N_2$), 7.80 (d, 2H, J = 9.6, $C_6H_4SO_3^-$), 7.71 (s, 2H, C_6H_4N), 7.71 (s, 2H, $C_6H_4SO_3^-$), 7.70 (d, 2H, J = 8.4 Hz, C_6H_4), 7.40 (d, 2H, J = 16.2 Hz, C_2H_2), 7.05 (d, 2H, J = 9.0 Hz, C_6H_4), 6.84 (d, 2H, J = 9.6 Hz, C_6H_4N), 4.50 (t, 1H, J = 4.8 Hz,

CH_3O), 4.03 (d, 2H, J = 13.2 Hz, CH_3O), 3.28 (t, 2H, J = 6.0 Hz, C_5H_9N), 3.06 (s, 6H, C_6H_4N), 2.91 (t, 2H, J = 12.6 Hz, C_5H_9N), 1.75 (d, 2H, J = 12.6 Hz, C_5H_9N), 1.66 (m, 1H, C_5H_9N), 1.19 (m, 2H, C_5H_9N). ^{13}C NMR (600 MHz, DMSO-d_6, δ): 160.11, 157.60, 154.70, 152.91, 152.55, 152.08, 149.20, 145.59, 142.58, 138.77, 131.50, 126.54, 124.79, 123.55, 122.85, 121.71, 121.18, 117.71, 113.98, 111.55, 65.57, 46.85, 38.29, 28.08. Elemental analysis for $C_{37}H_{39}N_7O_4S$: calcd. C 65.56, H 5.80, N 14.47, O 9.44, S 4.73; found: C 65.65, H 5.88, N 14.52, S 4.82.

4-(4-(4-(Hydroxymethyl)piperidin-1-yl)styryl)-1-(pyrimidin-2-yl)pyridin-1-ium 4-((4-(dimethylamino)phenyl)diazenyl)benzenesulfonate (PMPR-MO) from MO-Ag: First, (((4-((4-(dimethylamino)phenyl)diazenyl)phenyl)sulfonyl)oxy)silver (MO-Ag) was synthesized. MO-Na (1 g, 2.59 mmol) was dissolved in water (250 mL) at 55°C and silver nitrate (0.4 g, 2.59 mmol) was dissolved in water (60 mL). Two solutions were mixed and stirred at 55°C for 30 min. When two solutions were mixed, powder was immediately precipitated. After cooling to room temperature, the precipitated powder was obtained by filtration and dried in vacuum oven at 105 °C for ~10 h. Yield 75%. ^{1}H-NMR (600 MHz, DMSO-d_6, δ): 7.80 (d, 2H, J = 9.0 Hz, $C_6H_4SO_3Ag$), 7.72 (s, 2H, C_6H_4N), 7.72 (s, 2H, $C_6H_4SO_3Ag$), 6.84 (d, 1H, J = 9.6 Hz, C_6H_4), 3.07 (s, 6H, C_2H_6N). For synthesis of PMPR-MO, PMPR-Cl (0.3 g, 0.73 mmol) was dissolved in methanol (100 mL) and MO-Ag (0.3 g, 0.73 mmol) was dissolved in methanol (400 mL) at 55 °C. Two solutions were mixed and stirred at 55°C for 30 min. After cooling to room temperature, the precipitated AgCl was eliminated by filtration. The solvent in the residual solution was evaporated to ~200 mL at 50 °C. After cooling to room temperature, the solution was kept for 14 h. The precipitated powder was obtained by filtration (metathesis powder in Figure S1a). The final powder was obtained by recrystallization process in methanol and dried in vacuum oven at 105 °C for about 19 hours (crystalline Phase-I in Figure S1a). Yield = 40 %. ^{1}H-NMR (600 MHz, DMSO-d_6, δ) : 9.64 (d, 2H, J = 7.6 Hz, $C_5H_4N^+$), 9.16 (d, 2H, J = 4.8 Hz, $C_4H_3N_2$), 8.18 (d, 2H, J = 7.2 Hz, $C_5H_4N^+$), 8.16 (d, 1H, J = 14.4 Hz, C_2H_2), 7.87 (t, 1H, J =

4.8 Hz, $C_4H_3N_2$), 7.80 (d, 2H, *J* = 10.2, $C_6H_4SO_3^-$), 7.71 (s, 2H, C_6H_4N), 7.71 (s, 2H, $C_6H_4SO_3^-$), 7.70 (d, 2H, *J* = 9.6 Hz, C_6H_4), 7.05 (d, 2H, *J* = 9.0 Hz, C_6H_4), 6.84 (d, 2H, *J* = 9.6 Hz, C_6H_4N), 4.51 (t, 1H, *J* = 4.8 Hz, CH_3O), 4.03 (d, 2H, *J* = 13.2 Hz, CH_3O), 3.28 (t, 2H, *J* = 5.4 Hz, C_5H_9N), 3.07 (s, 6H, C_6H_4N), 2.91 (t, 2H, *J* = 12.0 Hz, C_5H_9N), 1.75 (d, 2H, *J* = 10.8 Hz, C_5H_9N), 1.66 (m, 1H, C_5H_9N), 1.19 (m, 2H, C_5H_9N). ^{13}C NMR (600 MHz, DMSO-d_6, δ): 160.11, 157.60, 154.71, 152.91, 152.56, 152.08, 149.21, 145.60, 142.59, 138.78, 131.51, 126.53, 124.79, 123.56, 122.86, 121.71, 121.18, 117.71, 113.98, 111.55, 65.57, 46.85, 38.29, 28.08. Elemental analysis for $C_{37}H_{39}N_7O_4S$: calcd. C 65.56, H 5.80, N 14.47, O 9.44, S 4.73; found: C 65.38, H 5.82, N 14.29, S 4.77.

4-(4-(4-(Hydroxymethyl)piperidin-1-yl)styryl)-1-(pyrimidin-2-yl)pyridin-1-ium 4-chlorobenzenesulfonate (PMPR-CBS): PMPR-Cl (1.5 g, 3.7 mmol) was dissolved in water (80 mL) at 55 °C and sodium 4-chlorobenzenesulfonate (CBS-Na, 1.6 g, 7.3 mmol) was dissolved in water (500 mL). Two solutions were mixed and stirred at 55°C for 30 min. After cooling to room temperature, the solution was kept for 14 h. The precipitated powder was obtained by filtration. The final powder was obtained by recrystallization process in ethanol and dried in vacuum oven at 105 °C for about 16 hours. Yield 77 %. ^1H-NMR (600 MHz, DMSO-d_6, δ): 9.64 (d, 2H, *J* = 7.6 Hz, $C_5H_4N^+$), 9.16 (d, 2H, *J* = 4.8 Hz, $C_4H_3N_2$), 8.18 (d, 2H, *J* = 7.2 Hz, $C_5H_4N^+$), 8.16 (d, 1H, *J* = 15.0 Hz, C_2H_2), 7.88 (t, 1H, *J* = 4.8 Hz, $C_4H_3N_2$), 7.70 (d, 2H, *J* = 9.0 Hz, C_6H_4), 7.59 (d, 2H, *J* = 8.4 Hz, $C_6H_4ClSO_3^-$), 7.40 (d, 1H, *J* = 16.2 Hz, C_2H_2), 7.37 (d, 2H, *J* = 9.0 Hz, $C_6H_4ClSO_3^-$), 7.05 (d, 2H, *J* = 9.0 Hz, C_6H_4), 4.50 (s, 1H, CH_3O), 4.03 (d, 2H, *J* = 13.1 Hz, CH_3O), 3.28 (t, 2H, *J* = 5.4Hz, C_5H_9N), 2.91 (t, 2H, *J* = 12.6 Hz, C_5H_9N), 1.75 (d, 2H, *J* = 12.6 Hz, C_5H_9N), 1.66 (m, 1H, C_5H_9N), 1.19 (m, 2H, C_5H_9N). ^{13}C NMR (600 MHz, DMSO-d_6, δ): 160.10, 157.58, 154.64, 152.89, 147.28, 145.57, 138.66, 132.98, 131.51, 127.72, 127.50, 123.52, 122.86, 121.74, 117.70, 113.94, 65.61, 46.84, 38.29, 28.10. Elemental analysis for $C_{29}H_{29}ClN_4O_4S$: calcd. C 61.64, H 5.17, Cl 6.27, N 9.91, O 11.33, S 5.67; found: C 61.43, H 5.22, N 10.05, S 5.89.

C. Crystal Structure Analysis of PMPR-MO (I) and PMPR-MO (II)

PMPR-MO (I): Single crystals of PMPR-MO (I) were grown in the first crystallization process (i.e., cooling method in methanol) of the metathesis powder based on MO-Na. $C_{23}H_{25}N_4O \cdot C_{14}H_{14}N_3O_3S$, M_r = 677.81, monoclinic, space group *Pc*, a = 12.7534(14) Å, b = 9.6747(11) Å, c = 14.4556(17) Å, β = 107.790(3)°, V = 1698.3(3) Å^3, Z = 2, T = 290(1) K, μ(MoKα)= 0.15 mm^{-1}. Of 12975 reflections collected in the θ range 3.3-25.0° using ω scans on a Rigaku R-axis Rapid S diffractometer, 5927 were unique reflections (R_{int} = 0.052). The structure was solved and refined against F^2 using SHELXL-2018/3, [G. M. Sheldrick, *Acta Cryst*. C71, 2015, 3] 443 variables, wR_2 = 0.172, R_1 = 0.059 ($F_o^2 > 2\sigma(F_o^2)$), GOF = 0.98, and max/min residual electron density 0.18/-0.14 eÅ^{-3}. CCDC-2101311.

PMPR-MO (II): Single crystals of PMPR-MO (II) were grown in the first crystallization process (i.e., cooling method in methanol) of the metathesis powder based on MO-Na. Note that PMPR-MO (II) single crystals were concomitantly grown with PMPR-MO (I) single crystals (CCDC-2101311). $C_{23}H_{25}N_4O \cdot C_{14}H_{14}N_3O_3S$, M_r = 677.81, triclinic, space group $P\bar{1}$, a = 9.3186(4) Å, b = 11.4401(6) Å, c = 16.5823(8) Å, α = 102.726(2)°, β = 93.598(1)°, γ = 104.112(1)°, V = 1659.58(14) Å^3, Z = 2, T = 290(1) K, μ(MoKα)= 0.15 mm^{-1}. Of 16458 reflections collected in the θ range 3.2-27.4° using ω scans on a Rigaku R-axis Rapid S diffractometer, 7503 were unique reflections (R_{int} = 0.039). The structure was solved and refined against F^2 using SHELXL-2018/3, [G. M. Sheldrick, *Acta Cryst*. C71, 2015, 3] 443 variables, wR_2 = 0.140, R_1 = 0.045 ($F_o^2 > 2\sigma(F_o^2)$), GOF = 0.92, and max/min residual electron density 0.35/-0.38 eÅ^{-3}. CCDC-2101310.

PMPR-MO (II): Single crystals of PMPR-MO (II) were grown in the second crystallization process (i.e., cooling method in methanol) of the metathesis powder based on MO-Ag. $C_{23}H_{25}N_4O \cdot C_{14}H_{14}N_3O_3S$, M_r = 677.81, triclinic, space group $P\bar{1}$, a = 9.3094(5) Å, b = 11.4328(7) Å, c = 16.5866(9) Å, α = 102.690(2)°, β = 93.554(1)°, γ = 104.264(2)°, V =

1656.50(16) $Å^3$, $Z = 2$, $T = 290(1)$ K, μ(MoKα)= 0.15 mm^{-1}. Of 16362 reflections collected in the θ range 3.2°-27.4° using ω scans on a Rigaku R-axis Rapid S diffractometer, 7440 were unique reflections (R_{int} = 0.036). The structure was solved and refined against F^2 using SHELXL-2018/3, [G. M. Sheldrick, *Acta Cryst*. C71, 2015, 3] 443 variables, $wR_2 = 0.169$, $R_1 = 0.047$ ($F_o^2 > 2\sigma(F_o^2)$), GOF = 1.11, and max/min residual electron density 0.42/-0.54 $eÅ^{-3}$. CCDC-2070574.

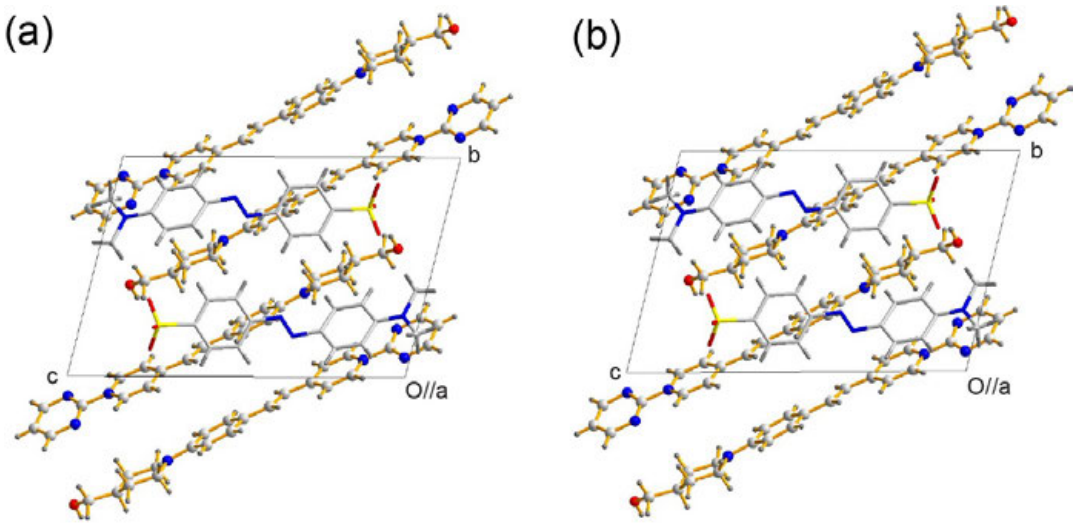

Figure S2. Molecular ordering of PMPR-MO (II) crystals with *P*-1 space group: (a) CCDC-2101310) from MO-Na and (b) CCDC-2070574 from MO-Ag.

D. Centrosymmetric Crystal Symmetry of PMPR-CBS Crystals

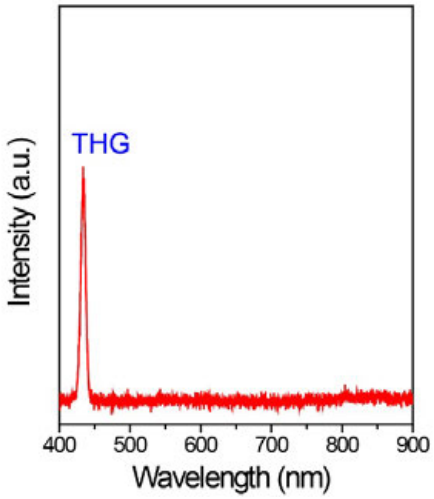

Figure S3. Powder second harmonic generation (SHG) experiments of PMPR-CBS at the fundamental pump wavelength of 1300 nm. No SHG signal was observed at 650 nm and only third harmonic generation (THG) signal at ~433 nm was observed. Therefore, PMPR-CBS crystals possess a centrosymmetric symmetry of molecular alignment in the crystalline state.

E. Molecular and Macroscopic Optical Nonlinearity

E.1 Previously Reported *N*-Pyrimidinyl Stilbazolium Crystals

Scheme 1b shows molecular optical nonlinearity of previously reported *N*-pyrimidinyl stilbazolium chromophores (OPR, HPR, ad DAPR) with various electron donating groups (EDGs). The maximum first hyperpolarizability β_{max} of optimized conformation (OPT) for DAPR chromophore was calculated using density functional theory with B3LYP functional and 6-311+G(d,p) basis sets following the literature. [*J. Phys. Chem. C* **2008**, *112,* 7846; *Adv. Funct. Mater.,* **2012***, 22,* 200] The maximum first hyperpolarizability β_{max} (OPT) for OPR and HPR that were calculated in same manner were obtained from Ref. [*Adv. Photonic. Res*., **2022**, *3*, 2100350 and *Opt. Laser Technol*., **2022**, 108454] The first hyperpolarizability β_{max} (OPT) of *N*-pyrimidinyl stilbazolium chromophores increases with increasing electron donating strength of electron donating groups (EDGs): 183, 228, and 281 × 10^{-30} esu for OPR, HPR, and DAPR, respectively.

To evaluate the macroscopic optical nonlinearity of OPR-, HPR-, and DAPR-based crystals, the effective first hyperpolarizability β_{ijk}^{eff} tensor was calculated by considering the crystal structure and the maximum first hyperpolarizability β_{max} of the experimental chromophore conformations (EXP) in crystals. The maximal diagonal components of the effective first hyperpolarizability β_{iii}^{eff} for OPR- and HPR-based crystals were obtained from Ref. [*Adv. Photonic. Res*., **2022**, *3*, 2100350 and *Opt. Laser Technol*., **2022**, 108454]: 204, 202, 192, 191, and 25 × 10^{-30} esu for OPR-EBS (4-(4-hydroxystyryl)-1-(pyrimidin-2-yl)pyridinium 4-ethylbenzenesulfonate), OPR-VBS (4-(4-hydroxystyryl)-1-(pyrimidin-2-yl)pyridinium 4-vinylbenzenesulfonate), OPR-T (4-(4-hydroxystyryl)-1-(pyrimidin-2-yl)pyridinium), OPR-CBS (4-(4-hydroxystyryl)-1-(pyrimidin-2-yl)pyridinium 4-chlorobenzenesulfonate), and HPR-N2S (4-(4-hydroxy-3-methoxystyryl)-1-(pyrimidin-2-yl)pyridin-1-ium naphthalene-2-sulfonate) crystals, respectively. For DAPR-based crystals, DAPR-T (4-(4-

(dimethylamino)styryl)-1-(pyrimidin-2-yl)pyridinium 4-methylbenzenesulfonate) crystals were chosen. [*Adv. Funct. Mater.* **2003***, 13,* 347] DAPR-T crystals exhibit centrosymmetric crystal space group and therefore all diagonal and off-diagonal components of the effective first hyperpolarizability β_{ijk}^{eff} tensor are zero for symmetry reasons.

E.2 Newly Designed PMPR-MO Crystals

The molecular optical nonlinearity of newly designed PMPR chromophore was calculated in the same manner as for previously reported crystals with B3LYP functional and 6-311+G(d,p) basis sets. [*J. Phys. Chem. C* **2008**, *112,* 7846; *Adv. Funct. Mater.,* **2012***, 22,* 200] The maximum first hyperpolarizability β_{max} (OPT) for PMPR chromophore is extremely large, 342 × 10^{-30} esu.

The diagonal component of the effective first hyperpolarizability β_{iii}^{eff} for PMPR-MO(I) crystals corresponding to the macroscopic optical nonlinearity is calculated by β_{max} (OPT)·$\cos^3\theta_{\text{p}}$, where the molecular ordering angle θ_{p} is the direction of the first hyperpolarizability β_{max} and the polar axis that is for symmetry reasons along the *ac*-crystallographic plane. For PMPR-MO(I) crystals, the direction of the maximum first hyperpolarizability β_{max} is considered along the direction between two N atoms on EDG and electron withdrawing group (EWG). The molecular ordering angle θ_{p} for PMPR-MO(I) crystals is about 7 degrees. The resulting diagonal component of the effective first hyperpolarizability β_{iii}^{eff} along the polar axis is crystals very large for PMPR-MO(I); 335 × 10^{-30} esu.

Note that for evaluation of the macroscopic optical nonlinearity for PMPR-MO(I) crystals in this work, the molecular optical nonlinearity of the MO anion was neglected. For the MO anion, the calculated maximum first hyperpolarizability are ca. 12 × 10^{-30} esu for the conformation in PMPR-MO(I) crystals (β_{max} (EXP)) and ca. 42 × 10^{-30} esu for the optimized conformation (β_{max} (OPT)), respectively. These β_{max} values for the MO anion show a very good agreement with previously reported values calculated by different methods. [*Opt. Mater*., **2019**,

94, 152] The maximum first hyperpolarizability β_{max} for the MO anion is one order of magnitude larger than that of conventional benzenesulfonate anions (e.g., β_{max} (OPT) = 3×10^{-30} esu for the CBS anion). However, the maximum first hyperpolarizability β_{max} for the MO anion is still one order of magnitude smaller than that of the PMPR chromophore (β_{max} (OPT) = 342×10^{-30} esu). In addition, the wavelength of maximum absorption λ_{max} for the MO anion is significantly shorter than that of the PMPR cation (see Figure 3b) and therefore also β_{max}, according to the conventional nonlinearity-transparency trade-off, [*Nonlinear Optical Effects and Materials*, (Ed: P. Günter), Springer-Verlag, Berlin, **2000**]. Consequently, the contribution of the optical nonlinearity of the MO anion is considered negligible for the macroscopic optical nonlinearity of PMPR-MO(I) crystals in this work.

In addition to using density functional theory calculations with crystal structure for evaluating the macroscopic optical nonlinearity, quantitative powder SHG measurements are also often employed to yield comparable results (see e.g. Fig. 15 in Ref. [*CrystEngComm*, **2016**, *18*, 7180]). However, in the crystallization processes for PMPR-MO (Figure S1), concomitant polymorphs with SHG-active PMPR-MO(I) and SHG-inactive PMPR-MO(II) were observed. Consequently, quantitative powder SHG measurements in this case cannot give reliable data for evaluating the macroscopic optical nonlinearity of the PMPR-MO(I) polymorph. Note that large second-order optical nonlinearity of PMPR-MO(I) crystals is proven by the extremely high THz wave generation efficiency in single crystals (Figure 4b and 4c).

F. Thermal Stability of PMPR-MO

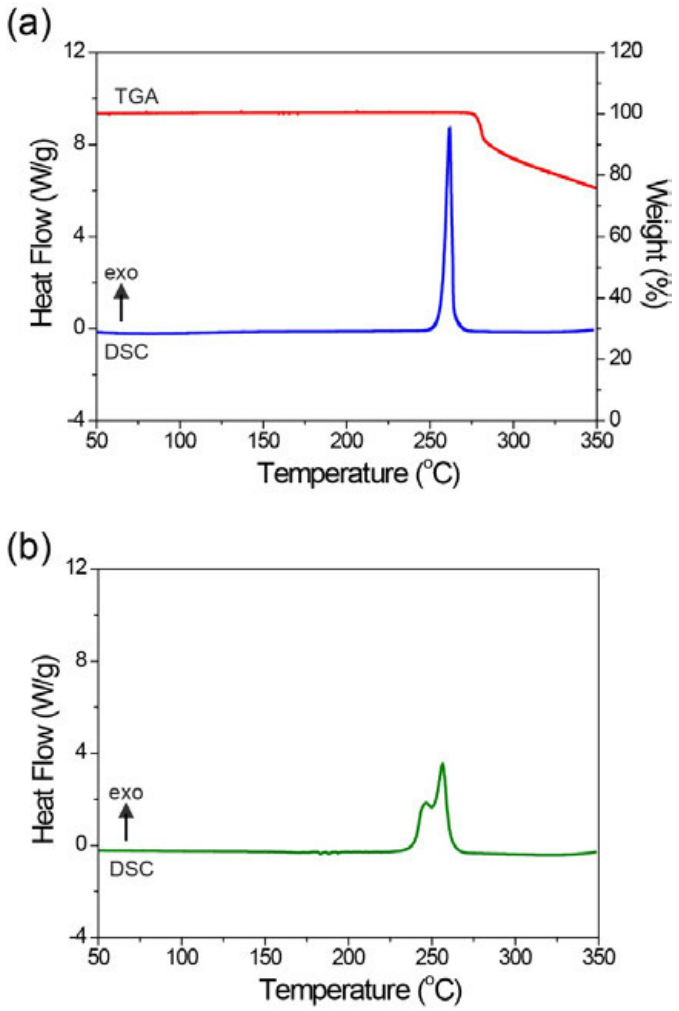

Figure S4. TGA and DSC thermodiagrams for PMPR-MO crystalline phases from MO-Ag: crystalline phase- (a) I and (b) II. PMPR-MO(I) exhibits a high thermal stability and no phase transition below the strong exothermic decomposition peak at ~ 260 ºC.

G. Morphology of As-grown PMPR-MO(I) Crystal

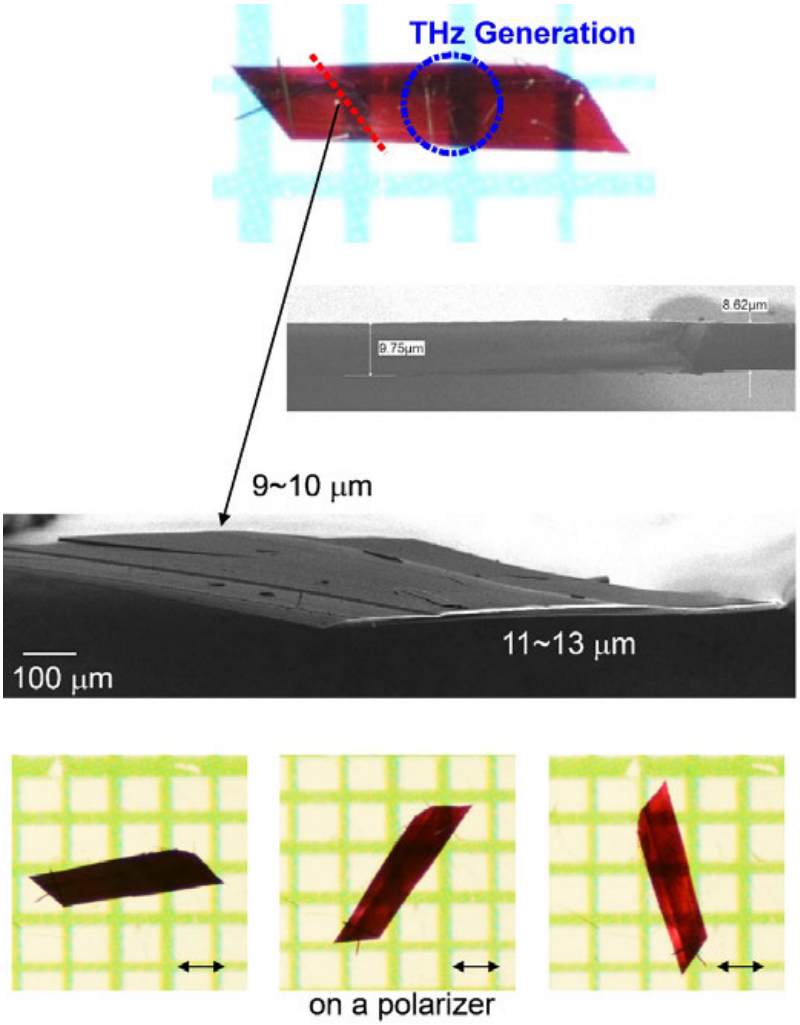

Figure S5. Ultra-thin PMPR-MO (I) crystal grown in the first crystallization process by cooling method in methanol solution (bottom: photographs on a polarizer). The blue dotted circle presents the area used for THz wave generation experiments in this work. The thickness of the crystal along the red dotted line is about 10 μm, as determined by scanning electron microscope (SEM) images. We assume that the thickness of the area used for THz generation experiments is very similar with that along the red dotted line. Consequently, we conclude that the overall thickness of the area used for THz wave generation experiments is about 10 μm. The as-grown crystals were not additionally processed (e.g., polished) for further experiments.

H. THz Wave Characteristics

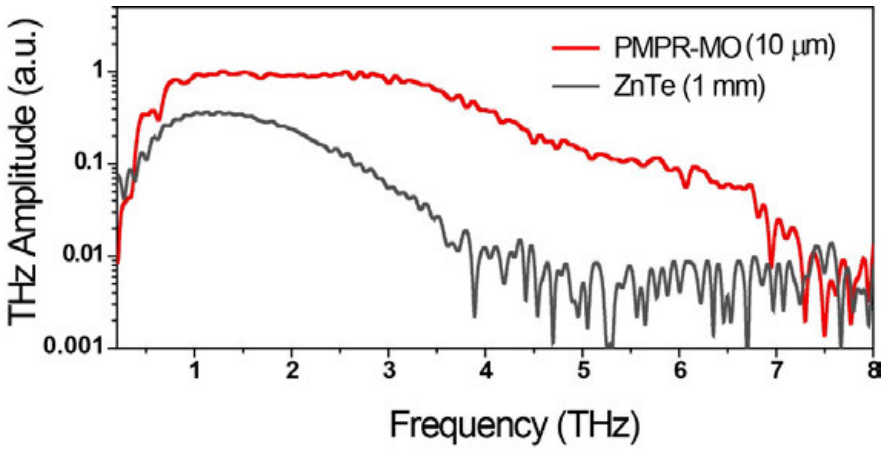

Figure S6. The generated THz generation spectra in a 10 μm-thick PMPR-MO(I) and in a 1.0 mm-thick ZnTe crystal, using optical pump pulses at 1300 nm.

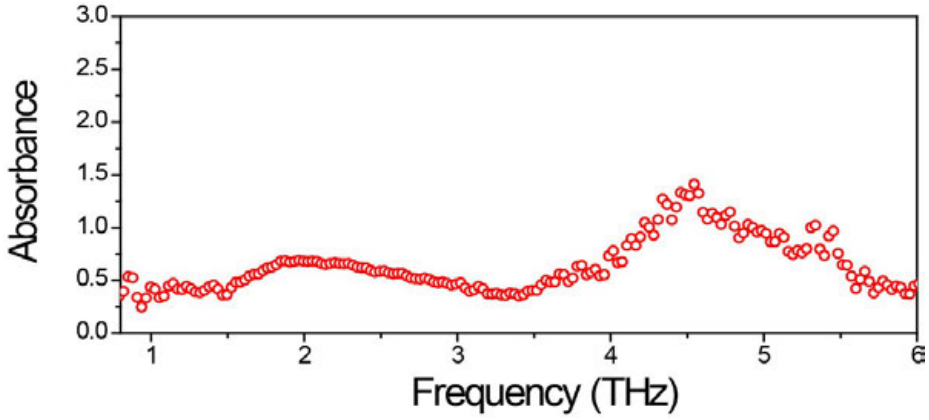

Figure S7. THz absorbance of a 10-μm-thick PMPR-MO(I) single crystal along the polar axis. The absorbance is defined as $-2\log_{10}T$ where T is the amplitude transmission of the THz electric field.

I. Hygroscopy Test

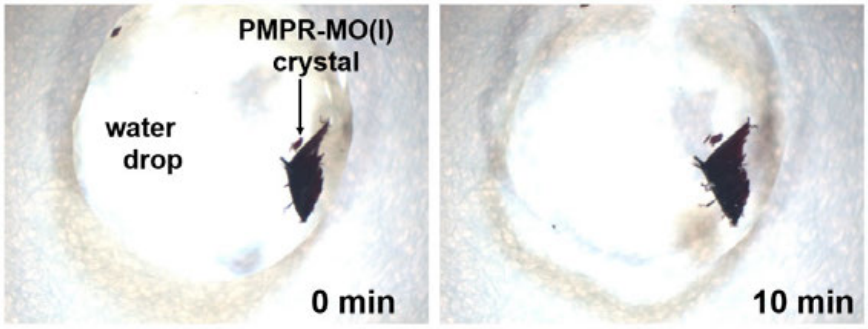

Figure S8. Hygroscopy test of PMPR-MO(I) crystal on a water droplet. After 10 min, PMPR-MO(I) crystal did not dissolve in water and the color of the water did not change.